



LAWRENCE
LIVERMORE
NATIONAL
LABORATORY

Simulating Picosecond X-ray Diffraction from shocked crystals by Post-processing Molecular Dynamics Calculations

G. Kimminau, B. Nagler, A. Higginbotham, W. Murphy,
N. Park, J. Hawreliak, K. Kadau, T. C. Germann, E. M.
Bringa, D. Kalantar, H. Lorenzana, B. Remington, J.
Wark

June 23, 2008

Journal of Physics: Condensed Matter

Disclaimer

This document was prepared as an account of work sponsored by an agency of the United States government. Neither the United States government nor Lawrence Livermore National Security, LLC, nor any of their employees makes any warranty, expressed or implied, or assumes any legal liability or responsibility for the accuracy, completeness, or usefulness of any information, apparatus, product, or process disclosed, or represents that its use would not infringe privately owned rights. Reference herein to any specific commercial product, process, or service by trade name, trademark, manufacturer, or otherwise does not necessarily constitute or imply its endorsement, recommendation, or favoring by the United States government or Lawrence Livermore National Security, LLC. The views and opinions of authors expressed herein do not necessarily state or reflect those of the United States government or Lawrence Livermore National Security, LLC, and shall not be used for advertising or product endorsement purposes.



Simulating Picosecond X-ray Diffraction from Shocked Crystals by Post-processing Molecular Dynamics Calculations

Giles Kimminau¹, Bob Nagler¹, Andrew Higginbotham¹, William J. Murphy¹, Nigel Park², James Hawreliak³, Kai Kadau⁴, Timothy C. Germann⁴, Eduardo M. Bringa⁵, Daniel H. Kalantar³, Hector E. Lorenzana³, Bruce A. Remington³, Justin S. Wark¹

¹Department of Physics, Clarendon Laboratory, University of Oxford, Parks Road, Oxford, OX1 3PU, UK

²AWE, Aldermaston, Reading, RG7 4PR, UK

³Lawrence Livermore National Laboratory, Livermore CA 94550

⁴Los Alamos National Laboratory, Los Alamos, New Mexico 87545, USA

⁵Univ. Nacional de Cuyo, Argentina

E-mail: giles.kimminau@physics.ox.ac.uk

Abstract. Calculations of the x-ray diffraction patterns from shocked crystals derived from the results of Non-Equilibrium-Molecular-Dynamics (NEMD) simulations are presented. The atomic coordinates predicted by the NEMD simulations combined with atomic form factors are used to generate a discrete distribution of electron density. A Fast-Fourier-Transform (FFT) of this distribution provides an image of the crystal in reciprocal space, which can be further processed to produce quantitative simulated data for direct comparison with experiments that employ picosecond x-ray diffraction from laser-irradiated crystalline targets.

PACS numbers: 31.15.xv,02.70.-c,02.30.Nw,61.05.C-,64.70.kd

1. Introduction

Non-Equilibrium Molecular-Dynamics (NEMD) simulations have started to provide exceptional insights into the atomistic behaviour of materials under shock compression. A significant amount of effort has concentrated on the study of the elastic-plastic transition within both single and polycrystalline materials [1, 2, 3, 4] as well as shock-induced polymorphic phase transitions [5, 6, 7]. In recent years, the impressive advances in computing power and storage space that have been made permit the size of such NEMD simulations to approach hundreds of millions (and in certain cases billions) of atoms, corresponding to samples of side-length approaching a micron, for simulated time-spans of up to hundreds of picoseconds [8, 9]. Given the vast amounts of data that can be generated by such simulations, a judicious choice of data-reduction and visualization systems is required in order to extract physical understanding from the raw data comprising the time-dependence of atomic coordinates. To date, most structural analysis has been limited to traditional short range methods

LLNL-JRNL-404855

such as obtaining radial distribution functions, centrosymmetry parameters [10] and coordination numbers.

However, simulations with these large spatial and temporal dimensions are starting to approach conditions found in experiments where matter, of thickness microns to several tens of microns, is shock compressed by high-power laser-matter interactions, and diagnosed by (amongst other techniques) *in situ* x-ray diffraction [11, 12]. These experiments have typically employed x-ray flashes of durations of several hundred picoseconds to a few nanoseconds, although picosecond resolution has been obtained by use of streak-camera technology [13], and laser-plasma x-ray sources with durations of order 100-fsec can now be produced routinely [14]. It is also expected that this field will benefit from the extremely bright femtosecond sources that will be afforded by future x-ray free-electron-laser technology [15].

As the NEMD simulations provide direct physical insight into the shock-deformation of materials at the lattice level, and the experimental and simulated time and length scales are converging, it is appropriate to make direct comparisons between the experimentally observed x-ray diffraction signals, and those predicted by the NEMD simulations. Indeed, such connections have started to be made: for example, Bringa and co-workers recently used NEMD simulations to calculate the shift in both the Bragg (reflected) and Laue (transmitted) peaks in shock-compressed copper [8], which were directly related to the time-dependent shape of the unit cell, and via this provided information regarding the degree of plastic flow. Hawreliak *et al.* directly compared the diffraction patterns predicted by NEMD with the experimental data for the $\alpha - \epsilon$ transition in shocked iron, noting, amongst many other things, good agreement between the predicted x-ray line widths in the ϵ phase and those seen experimentally - an observation which is consistent with the predicted mean size of two families of domains with orthogonal c -axes [12]. However, whilst simulated diffraction patterns have been presented, to date the procedure by which one can take the output of a NEMD simulation and produce quantitative predictions of what will be observed in an experiment has not been discussed in any detail. In this paper we present such an analysis, outlining how to post-process the NEMD data to efficiently produce diffraction patterns that can be directly compared with data obtained in commonly-employed experimental geometries.

2. Calculation of Reciprocal Space

Neglecting the effects of absorption, and in the kinematic approximation, when an x-ray of wavevector \mathbf{k}_0 is incident on a crystal, the intensity $I(\mathbf{k}_s)$ of the elastically scattered x-ray of wavevector $\mathbf{k}_s = \mathbf{k}_0 + \mathbf{q}$ is proportional to the modulus-squared of the Fourier-component of the electron density of the lattice with reciprocal lattice vector \mathbf{q} . If, in a very simplified approach, we represent the atoms by point scatterers located at the spatial coordinates provided by the MD simulation, then the scattered intensity is given by

$$I(\mathbf{k}_s) \propto |F(\mathbf{q})|^2 \propto \left| \sum_{j=1}^N Z_j \exp(i\mathbf{q} \cdot \mathbf{r}_j) \right|^2, \quad (1)$$

where Z_j is the atomic number of the j -th atom, located at position \mathbf{r}_j , and the sum is over all N atoms within the crystal. Whilst such a simple calculation can be of use in sampling specifically defined regions of reciprocal space which require the calculation

of a very limited number of Fourier components (for example, a volume around a particular Bragg peak), it is inefficient when applied to calculations of the full range of reciprocal space due to the $O(N^2)$ computational operations required. Information about the full range of reciprocal space is potentially useful in many situations: for example to understand the polycrystalline response to shock compression, or to single crystal analysis where the large defect densities generated may give rise to significant scattering between the Bragg peaks.

Likewise performing an FT by this method is also sensible when the number of atoms is small. However, it is because the number of atoms in modern NEMD simulations is so large that this becomes prohibitive. While there is plenty of useful information to be gained from small scale equilibrium MD simulations, applications such as shock waves often require very large spatial and temporal dimensions in order not to hinder effects such as defect motion and to avoid reflection from the boundaries. In such NEMD simulations, the initial system, usually a perfect single crystal or a many grained polycrystal, is thermalised under equilibrium conditions before being deformed. As shock waves are assumed to be adiabatic there is no additional coupling of the atoms to a heat bath in NEMD.

In order to calculate reciprocal space from a large scale NEMD simulation we need a more efficient means of performing the Fourier Transform than that given in Eq (1). The method we employ is the Fast Fourier Transform (FFT) approach, the details of which are well known and will not be repeated here, save to recall that an FFT is an efficient method to compute a Discrete Fourier Transform (DFT) in $O(N \log_2 N)$ operations rather than $O(N^2)$. Whereas the summation used in the simple method of Eq (1) exploited the fact that the position vectors of the atoms provided by the MD simulations could be used directly as delta functions, a DFT requires an evenly spaced sample array in real space, making it unsuitable. However, atomic coordinates from the MD actually represent the centres of atoms which have a spatially extended electron distribution. By associating an electron distribution with each atomic coordinate we can construct a discrete regular array of electron density upon which we can perform the FFT.

Calculations of spherically-symmetric electron distributions for the elements are available from a number of sources [16]. Certain very simple analytic forms exist which represent the distributions in real space as a sum of a finite number of Gaussian profiles [17]. The Fourier transform of these radial distributions, the atomic form factors, are also available based on a number of approximations, such as the Thomas-Fermi or Dirac-Fock methods [16], and we use such forms here for the quantitative calculation of diffraction patterns.

Once an electron distribution has been associated with each atomic coordinate, the level of real space sampling is determined by the range of interest in reciprocal space, with the number of samples per unit cell in real space determining the range of the transformation in reciprocal space. For example, if we wish to explore reciprocal space out to the fifth order (based on a conventional unit cell in real space) then we require a range of at least 10 reciprocal lattice vectors, corresponding to 10 samples per side of a conventional unit cell, i.e. 10^3 over the conventional cell volume. On the other hand the resolution in reciprocal space is determined by the number of unit cells in the MD calculation, and hence the requirement for large MD simulations if we wish to have high resolution in reciprocal space, and in the resultant calculated diffraction patterns.

Although we can use the physical electron distribution to calculate a realistic array of electron density, it is advantageous to exploit this method for greater efficiency. Difficulties arise because of the interplay between the width of the electron distribution in real space and the radial extent of the intensity of the Fourier components in reciprocal space. If the spatial profile is too narrow, the Fourier components in reciprocal space could still have significant amplitude at the edges of the chosen range of reciprocal space, resulting in the pattern being reflected back (as FFTs are periodic), or overlapping, which is known as aliasing. On the other hand, too wide a profile in real space for a chosen range of reciprocal space implies that the intensity of high orders in reciprocal space will be too weak, and information may be lost. In cases where we have selected a specific range of reciprocal space, we have found it useful to choose a Gaussian profile in real space such that the 4σ position of the Gaussian envelope (amplitude) in reciprocal space lies on the edge of the reciprocal space array. Thus we are no longer assigning a physical electron density, but are instead ‘dressing’ each atomic coordinate with a Gaussian which allows us optimal control.

The approach of ‘dressing’ each atomic coordinate works due to the relationship of a convolution in real space and multiplication in reciprocal space. The Fourier transform of the real-space convolution of the atomic distribution function with a Gaussian electron density is just the product of the Fourier transforms of the atomic distribution function and the Gaussian profile. Therefore, the Fourier transform of the atomic distribution function with a physically realistic electron density function is just:

$$\begin{aligned} \mathcal{F}[ADF \otimes \rho(r)] &= \mathcal{F}[ADF \otimes G(r)] \times \frac{\mathcal{F}[\rho(r)]}{\mathcal{F}[G(r)]} \\ &= \mathcal{F}[ADF \otimes G(r)] \times \frac{F(k)}{\tilde{G}(k)} \quad , \end{aligned} \tag{2}$$

where \mathcal{F} is the Fourier transform operator, ADF is the atomic distribution function which is simply a delta function placed at each of atomic coordinates taken from MD, $\rho(r)$ is the electron density for one atom, $G(r)$ is the Gaussian profile of our choosing in real space and hence $\tilde{G}(k)$ is the Fourier transform of it and $F(k)$ is the atomic form factor which is the Fourier transform of $\rho(r)$.

By exploiting the properties of Fourier transforms, using a non-physical radial electron density in this way for convenience does not compromise the physical validity of the calculation. By using a convenient Gaussian atomic electron density of known width, we avoid aliasing, and we are able to infer the FFT of the atomic distribution. After performing the FFT of the atomic distribution function convolved with the Gaussian profile we can then divide by the Fourier transform of the Gaussian profile (which we know analytically) to give us the FFT of the atomic distribution function. We then proceed to multiply by the atomic form factor which produces output equivalent to using the physically realistic electron density in the first place, as shown in Eq (2).

It is evident that evaluating reciprocal space at high orders increases the size of the calculation significantly, but given the number of atoms involved, the FFT is still a more computationally efficient means of viewing reciprocal space compared with the normal FT, unless only a very small sub-set of reciprocal space is of interest. For example, calculating reciprocal space up to 5^{th} order from several million atoms can be computed in a matter of minutes on a typical workstation. The main limitation of

the FFT method is the memory usage which is around 4GB per million unit cells if calculating reciprocal space up to 5th order at single precision. Large shared memory machines are particularly well suited to calculating FFTs of 10s or 100s of millions of atoms. The method also works on MPI (Message Passing Interface) clusters, but with the disadvantage of requiring extra memory for the FFT transposes and node overhead. However, for analysis of MD simulations, it is often desirable to calculate reciprocal space with some spatial resolution, and, as such, the sample can be divided up into sections which can be calculated quickly on single nodes. Likewise on polycrystalline or highly defected samples where it may be necessary to gain information about the entire sample, the reciprocal peaks are often broad enough to allow a lower resolution, and hence the intensities of smaller FFTs can be summed.

3. Quantitative Calculations

In section 4 we will show how we can post-process the representation of the crystal in reciprocal space to obtain simulated diffraction patterns for specific experimental geometries. This processing is reliant on the fact that the intensity of the scattered radiation is proportional to the square of the relevant Fourier component, as stated in eqn (1).

Although the spatial scales of MD simulations are starting to converge, it is still generally the case that experiments use crystals of thickness between one and two orders of magnitude greater than the simulations. Furthermore, there could often be situations where due to constraints on computational resources it is desirable to perform a simulation that has a spatial scale significantly smaller than that used in an experiment, yet there is a requirement to have some predictive capability for the experimental intensity to compare with features in the simulations. Therefore, in order to have a means estimating what intensities might actually be found in an experiment, we need to associate each value of $|F(\mathbf{q})|^2$ in reciprocal space with a reflectivity that corresponds to that which may be expected in the experimental configuration.

Such an association can be made by noting that the efficiency of scattering from a single atom is known. If unpolarized X-rays of wavevector \mathbf{k}_0 are incident on a single atom, and are elastically scattered into wavevector $\mathbf{k}_s = \mathbf{k}_0 + \mathbf{q}$, then the differential cross-section, $d\sigma/d\Omega$ is given by

$$\frac{d\sigma}{d\Omega} = r_e^2 \frac{(1 + \cos^2 \theta)}{2} f^2(|\mathbf{q}|, Z) \quad , \quad (3)$$

where r_e is the classical radius of an electron, θ is the angle of deflection and $f(|\mathbf{q}|, Z)$ is the atomic form factor for element Z , which is proportional to the Fourier transform of the spherically-symmetric electronic density distribution discussed in section 2. Let us consider the case where we have performed an NEMD simulation of a crystal which contains N atoms,

$$\frac{d\sigma}{d\Omega} = r_e^2 \frac{(1 + \cos^2 \theta)}{2} \left| \sum_{i=1}^N f_i(|\mathbf{q}|, Z) e^{i\mathbf{q}\cdot\mathbf{r}_i} \right|^2 \quad . \quad (4)$$

We note that if our system has only one type of atom the atomic form factor can be separated out

$$\frac{d\sigma}{d\Omega} = r_e^2 \frac{(1 + \cos^2 \theta)}{2} f^2(|\mathbf{q}|, Z) \left| \sum_{i=1}^N e^{i\mathbf{q}\cdot\mathbf{r}_i} \right|^2 \quad , \quad (5)$$

and in this particular case we can easily remove the effect of the form factor after performing the FFT by deconvolution with the Gaussian in Fourier space associated with the form factor. Absolute intensities can be obtained by noting that as the electron density is real, the rms value of the electron density within the system is not a function of the correlations. This means that the integral of the intensity of Fourier components of the electron density over the whole of reciprocal space is a constant for a given number of atoms in a fixed volume. This is simply a form of Parseval's theorem which provides us with a means of normalizing the intensity of the components in reciprocal space, such that a given intensity density in reciprocal space corresponds to a quantitative measure of the scattered x-ray intensity.

This approach both neglects absorption within the crystal (and thus would not be valid for crystal thicknesses approaching or exceeding an absorption depth), and neglects the effect of extinction - that is to say re-scattering within the crystal. The proper handling of extinction effects require wave-wave interactions that are described by dynamical diffraction theory. The assumption of kinematic diffraction is likely to be valid for crystals containing large numbers of defects, or large strain gradients, as is the case in the shocked samples considered here. It may, however, not be a valid assumption for diffraction from large unshocked regions of the crystal if the sample has a high degree of perfection.

We can thus, using the above approach, calculate (within the approximations given) an absolute scattered x-ray fraction from the MD simulation. Furthermore, it is now simple to scale a calculated intensity. That is to say based on a simulation of a small system, we can infer the intensity that would be scattered in a larger system (as long as the path lengths of the scattered rays do not traverse distances greater than of order an absorption depth), as the intensity in this case is directly proportional to sample thickness. Of course, it may be that the physics of the MD simulation in question cannot be scaled linearly, but that is a separate matter from the diffraction calculation.

4. Experimental diffraction geometries

4.1. Single Crystal Diffraction

One of the primary motivations for this work is to enable the comparison of the predictions of MD simulations with picosecond x-ray diffraction from laser-shocked crystals. Once the FFT has been performed, and we have the values for the intensities of the Fourier components $|F(\mathbf{q})|^2$ in reciprocal lattice space (and know how these can be translated into scattering cross-sections for an experimental sample), we can proceed to calculate the pattern observed experimentally. Our intent in this paper is to outline how such calculations are performed, and give example output alongside experimental results. We do not, however, go into detail concerning the physics that may be gleaned from these comparisons, leaving such discussions for future work dedicated to that specific purpose.

One of the most widely used experimental geometries for picosecond diffraction from shocked crystals has been the diverging beam geometry [18], described by Kalantar and co-workers [19] and explained in more detail in the appendix. In this geometry, shown schematically in Fig. 1, the output of a high-power ns optical laser is focused onto a thin foil, generating a highly ionized plasma which in turn emits a short pulse of quasi-monochromatic x-rays. The x-ray source is approximated as

an isotropic point-source for this simulation. Another laser beam is used to drive the shock-wave in the crystal by ablating the front surface. The x-rays penetrate far enough into the crystal to diffract from the regions both in front and behind the shock front and the resulting lines are recorded on the surrounding film packs.

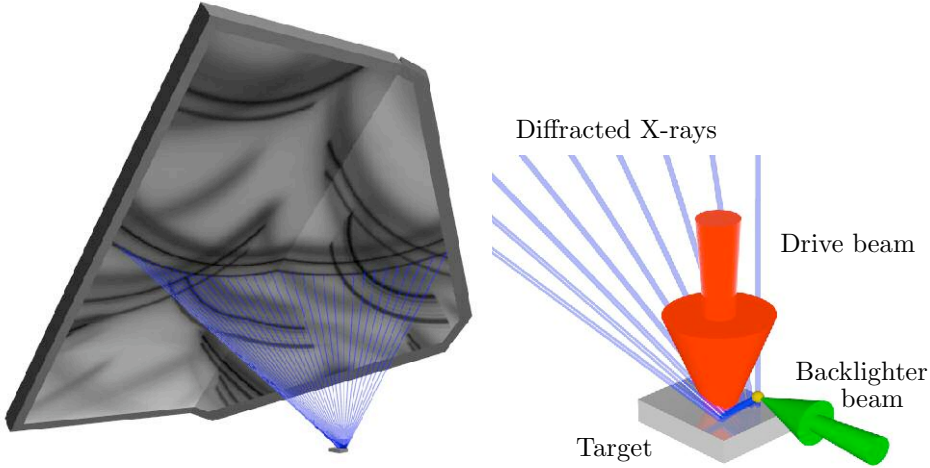


Figure 1. Experimental setup of single crystal diffraction from a diverging x-ray point source. For illustration the path of some x-rays of 1.85\AA diffracting from the (002) plane of Fe are shown.

To calculate the intensity incident on the film and hence the number of photons per pixel, we sample the film by ray-tracing back to the point source using the Laue formalism: $\mathbf{q} = \Delta\mathbf{k} = \mathbf{k}_s - \mathbf{k}_0$, where \mathbf{k}_0 is the incident wave vector, \mathbf{k}_s the diffracted wave vector and \mathbf{q} a vector in reciprocal space with known scattering intensity.

For each sample on the film, x-rays can arrive via any point on the crystal surface and as such the entire crystal needs to be well sampled for each film sample. We do this by dividing up our crystal in the surface plane into an array of sub crystals, each of which is illuminated by a collimated beam and hence corresponds to a single sample in reciprocal space per film sample. Obviously the sub-crystal must be small enough to be reasonably represented by a single reciprocal space sample which in turn can be found by linearly interpolating our FFT output and multiplying by the appropriate coefficients to calculate the cross-section. One advantage of sampling (as opposed to photon mapping) in both the film and crystal planes is that the sampling need not be uniform which can improve efficiency in certain situations.

As an example of this procedure we have simulated the diffraction from a single crystal of iron shocked along the [001] axis. The NEMD simulation was performed using the SPaSM code [20, 21] with the Voter-Chen potential [22]. A sample with dimensions $40.2\text{nm} \times 40.2\text{nm} \times 57.4\text{nm}$ consisting of 8 million atoms were launched along the [001] direction at a velocity of 471ms^{-1} into a momentum mirror. Previous work using this potential have shown that at this particle velocity the iron undergoes a transition from the body-centred-cubic α phase into the hexagonal-close-packed ϵ phase. An image of the crystal after a simulation time of 8.46ps is shown in Fig. 2, where the atoms are coloured according to coordination number. Here we can clearly

see the 3 distinct sections consisting of the unshocked region coloured grey (right), the uniaxially compressed region in blue (middle) and the phase changed region in red (left). For further detail about the simulation one should refer to the original work [6].

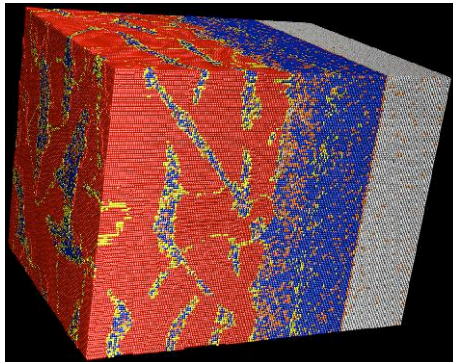


Figure 2. MD simulation of Fe shocked along [001] at 471ms^{-1} . Atoms are coloured according to coordination number displaying the unshocked region coloured grey (right), the uniaxially compressed region in blue (middle) and the phase changed region in red (left). From [6]. Reprinted with permission from AAAS.

Using the atomic coordinates provided by the MD simulation, the diffraction pattern was calculated according to the procedure described above. The reciprocal space was calculated by using a real-space matrix of $1024 \times 1024 \times 1458$ and hence requiring 6GB of memory. This generated reciprocal space beyond $3.2 \frac{2\pi}{a}$ which is the highest order experimentally accessible using Fe He- α X-rays at 1.85\AA . This contains 140 samples per reciprocal unit cell in the x and y directions and 187 in the z direction corresponding to the number of unit cells in each dimension. We set the origin of our world coordinates to be the position of the x-ray point source and define the crystal to be in the x-y plane, centred at (0,1.5, -1)mm. The crystal is $3 \times 3\text{mm}$ in extent with the crystallographic axis rotated by 13° around [001] to the world axis. In order to calculate the absolute intensities we assumed the crystal had a thickness of $10\mu\text{m}$ as in the experiment. The film packs are then positioned 60mm away with the normal along the [011] direction. The main rectangle is 130mm in the [011] direction and 65mm along [100]. The triangular pack (used in the experiments) is then positioned adjacent to this with the same extents but rotated inwards by 60° . Some minor rotations and offsets are then performed in order to fit the simulation to the exact experimental geometry. To produce this figure the film was sampled at $200\mu\text{m}$ and the crystal surface at $50\mu\text{m}$ resolution. Generating reciprocal space from an ASCII file containing atomic coordinates took 3 minutes and the tracing took 40 minutes on an 8-core Xeon Mac Pro. Lower quality but still meaningful figures can be traced in a fraction of the time.

The simulated diffraction pattern is shown in Fig. 3 next to an example of experimental data taken on the Vulcan laser [23] under experimental conditions very similar to the work performed by Kalantar and co-workers [11]. The Fe single crystal was coated with $20\mu\text{m}$ of parylene-N and driven with a 230J pulse at 1053nm and 6ns duration. The x-ray source was generated with a 1ns pulse of approximately 150J at 527nm, delayed by 4.5ns with respect to the drive pulse. On both the simulated and

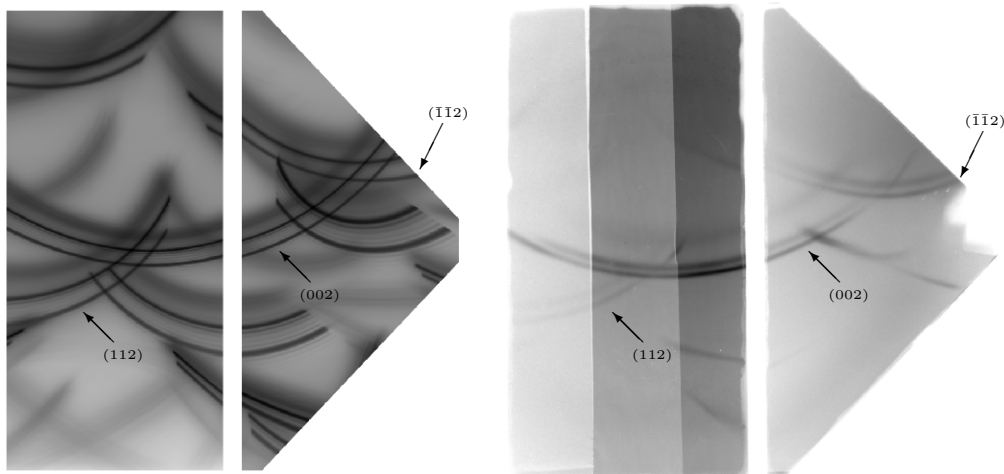


Figure 3. Simulated (left) and experimental (right) film recordings of x-rays diffracted from shock compressed iron. See text for details. Both clearly show the unshocked, uniaxially compressed and phase changed lines. Miller indices for several reflections are indicated. The plotted intensity is logarithmic for the simulated diffraction with a range of 5 orders of magnitude with a maximum number of photons per unit area of $3 \times 10^{-3} \text{ m}^{-2}$ of the total number emitted by the source in the Helium alpha line.

experimental diffraction patterns the 3 lines corresponding to unshocked, uniaxially compressed and phase changed lattice are clearly visible. This allows a direct comparison of NEMD simulations with experimental results. Even without detailed analysis we can clearly see that the strain in the uniaxially compressed region differs significantly between the NEMD simulation and the experiment from the position of the line while the unshocked and HCP lines either side match well. The line widths of the HCP features in the simulated and experimental data are comparable and the peak intensities are within an order of magnitude (after background subtraction) if we assume an x-ray conversion efficiency of 10^{-3} and sensitivity for Fujifilm MS type-image plate of around 100 photons per unit PSL per pixel [24]. Given that the image plate has a sensitivity of 5 orders of magnitude [25] and the images displayed are logarithmic, we conclude that the estimated absolute intensities that would be recorded are sufficiently accurate to aid in the design of experiments.

4.2. Polycrystalline Diffraction

Although many experiments involving picosecond diffraction from shocked materials have been performed with single crystals, it has recently been shown that single shot diffraction patterns can be obtained from polycrystalline samples using laser-plasma x-ray sources [26]. In this case, a collimated beam of quasi-monochromatic radiation, once more produced from the resonance lines of Helium-like atoms, is incident on a foil of polycrystalline metal. In the experimental work of Hawreliak *et al*, the source to foil distance was 5 cm, and the diffracted x-rays were recorded on a cylindrical film pack co-axial with the incident x-rays. Here we simulate an experiment of similar

dimensions, though we place a planar film pack behind the target in a normal Debye-Scherrer geometry, with similar target to film distances as those used in the experiment (conversion to a cylindrical film pack geometry provides no extra information). The geometry is shown in schematic form in Fig. 4.

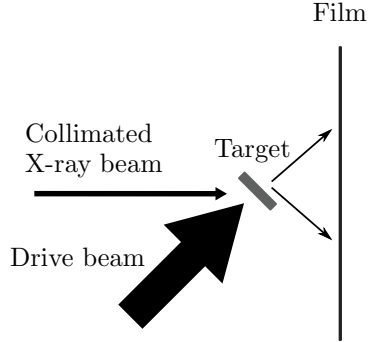


Figure 4. Polycrystalline experimental setup

In terms of the post-processing of the reciprocal space data, we note that in this case the direction of the incident beam is fixed, and its orientation with respect to the reciprocal space axes is simply determined by the angle ψ which the surface normal of the foil makes to the incident beam. In this case the experimentally observed diffraction pattern is determined by the angle of the \mathbf{k}_s vector as \mathbf{k}_0 is fixed in direction by the collimation and in magnitude by the monochromatic nature of the source. As a result, \mathbf{k}_s traces out a shell in reciprocal space which touches the origin. This in turn intersects the shells of \mathbf{G}_{hkl} of strong reflections, which are centred at the origin, resulting in a pattern of rings on film - the well known Debye-Scherrer pattern.

In our calculations the crystal surface is placed at 45° to the collimated X-ray beam. This allows the shell that is traced out by \mathbf{k}_s to intersect both the x-y components (orthogonal to shock) and the z-components (shock direction) of the \mathbf{G}_{hkl} shells and hence give an indication of the level of compression along different crystal axes.

As an example of this procedure we have simulated the diffraction from a polycrystal sample of Cu with X-rays of wavelength 1.48\AA . The NEMD simulation was performed using the LAMMPS package [27] using the Mishin EAM1 potential [28]. A sample with dimensions $72\text{nm} \times 72\text{nm} \times 72\text{nm}$ consisting of 30 million atoms in approximately 3000 grains was used. The initial sample was created with the Atomeye utilities [29] before undergoing energy minimisation by the conjugate gradient algorithm and thermalisation at 300K. A piston was set moving into the sample at 900ms^{-1} and the simulation was run for 15ps to allow the shock wave to travel the full extent of the sample which compressed by approximately 20% volumetrically.

In order to compare diffracted intensities with those observed experimentally, it was assumed that the illuminated sample is a foil $25\mu\text{m}$ thick and 1mm square. The diffraction was traced in the same manner as the single crystal case except that as the beam is collimated only one sample on the crystal is needed for every sample of the film. The target was placed 50mm from an x-ray point source and the beam approximated as collimated. The $12 \times 12\text{cm}$ film was then placed 15mm from the

sample. The FFT was performed using 8 processors and 32 GB of RAM on an SGI Altix 4700 in 26 minutes with the tracing taking seconds.

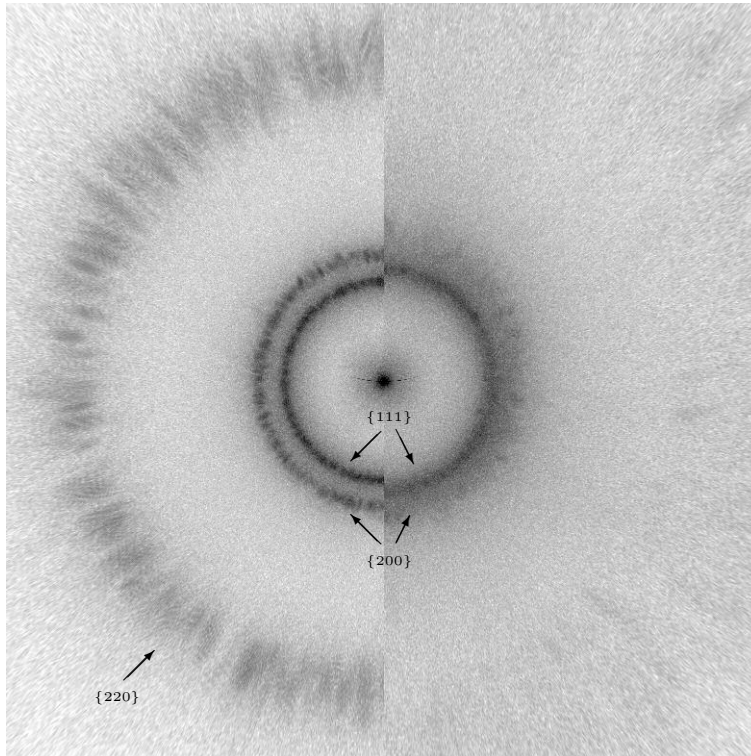


Figure 5. Simulated diffraction from polycrystalline Cu. The figure is split with the left side showing diffraction from the unshocked crystal and the right hand side from the same crystal but shocked at 900ms^{-1} . The plotted intensity is logarithmic with a range of 5 orders of magnitude with a maximum number of photons per unit area of 10^{-5} m^{-2} of the total number emitted by the source in the Helium alpha line. See text for further details.

The diffraction patterns for both the unshocked (left) and shocked(right) foils are shown in Fig. 5. The maximum intensity observed is once more within an order of magnitude of those found in experiments. The expansion of the diffraction rings due to a compression of the lattice is clearly visible in the shocked sample.

5. Summary

We have presented calculations of the x-ray diffraction patterns from shocked crystals derived from the results of Non-Equilibrium-Molecular-Dynamics (NEMD) simulations. The atomic coordinates predicted by the NEMD simulations combined with atomic form factors are used to generate a discrete array of electron density. A Fast-Fourier-Transform (FFT) of this array provides an image of the crystal in reciprocal space, which can be further processed to produce simulated quantitative data for direct comparison with experiments that employ picosecond x-ray diffraction from laser-irradiated crystalline targets. Estimates of absolute intensities that may be

observed in real experiments have been obtained from a knowledge of x-ray scattering cross-sections, and scaling the intensity scattered by the MD predictions accordingly. Good agreement is found between computed and experimental diffraction patterns, and the technique should be useful in both designing novel experiments, as well as in analysis of the signals obtained by using of picosecond diffraction from shocked crystals.

6. Acknowledgments

The authors are grateful to a number of organizations for support. G.K is grateful for partial support for this work from LLNL under subcontract No. B566832. B.N is supported by the EU Marie-Curie RTN ‘FLASH’. J.H, D.K, H.L and B.R work under the auspices of the U.S. DOE by LLNL under Contract DE-AC52-07NA27344. H.L. and J.H. also received partial support from LDRD program Project No. 06-SI-004 at LLNL. W.J.M. is grateful for support from AWE Aldermaston. A.H. has been generously supported by Daresbury Laboratory under the auspices of the NorthWest Science Fund. K.K. and T.G. work under the auspices of the National Nuclear Security Administration of the U.S. Department of Energy at Los Alamos National Laboratory under Contract No. DE-AC52-06NA25396. We also wish to thank P.S. Lomdahl and B.L. Holian for valuable discussions. Simulations were performed on the QUEEG and ORAC machines at the Oxford Supercomputing Centre.

7. Appendix: Experimental Geometry

In the diverging beam geometry, shown schematically in Fig. 1, a short pulse of x-rays is generated by focussing the output of a high-power ns optical laser onto a thin foil. The laser intensities are such that a highly ionized plasma is formed, and copious x-rays are produced. Depending upon the element used, for laser intensities in the range of 10^{14} to 10^{16} W cm⁻², a significant fraction of the radiation is emitted in the $n = 2 \rightarrow 1$ resonance line of the Helium-like ion. These x-rays are quasi-monochromatic in that alongside the resonance line itself, which corresponds to the $1s2p^1P \rightarrow 1s^2^1S$ transition, in the plasma environment there is also significant emission in the intercombination line, $1s2p^3P \rightarrow 1s^2^1S$, as well as emission into dielectronic satellites. The fractional bandwidth of these transitions taken together is of order 5×10^{-3} . Typical conversion efficiencies from optical laser light into these lines is of order 10^{-2} to 10^{-4} [30, 31], and typical source diameters are of order 100 μ m.

The x-rays that are emitted from the hot plasma diverge into 4π steradians. Therefore, in order to maximize the information gleaned from diffracting from the shocked crystal, the x-ray source is placed close to the crystal (with typical source to crystal distances of order 1 mm), such that the shocked crystal subtends a relatively large solid angle to the x-ray source. The diameter of the region of the crystal which is shocked by the laser, determined largely by considerations of the laser energy, is typically of order 3 mm. X-rays diffracted from the shocked crystal are recorded on large area flat film packs placed several cm from the crystal, which are arranged to cover as large a solid angle as possible given the constraints imposed by experimental considerations such as the need to provide access for the optical laser beams. When the surface layer of thick crystals are shocked, the diffracted radiation is collected in the reflection geometry (so-called Bragg diffraction). Experiments with thin crystals, with

thicknesses of order $10\mu\text{m}$, have also simultaneously allowed diffraction in transmission geometry (so-called Laue diffraction). The scattered x-rays are recorded on either x-ray film or image plates. The direct path between the x-ray source and film packs is obscured by highly absorbing beam blocks.

References

- [1] Y.M. Gupta. Effect of crystal orientation on dynamic strength of LiF. *Journal of Applied Physics*, 48:5067, 1977.
- [2] B.L. Holian and P.S. Lomdahl. Plasticity Induced by Shock Waves in Nonequilibrium Molecular-Dynamics Simulations. *Science*, 280(5372):2085, 1998.
- [3] EM Bringa. Atomistic shock Hugoniot simulation of single-crystal copper. *Journal of Applied Physics*, 96(7):3793, 2004.
- [4] Eduardo M. Bringa, Alfredo Caro, Yinmin Wang, Maximo Victoria, James M. McNaney, Bruce A. Remington, Raymond F. Smith, Ben R. Torralva, and Helena Van Swygenhoven. Ultrahigh Strength in Nanocrystalline Materials Under Shock Loading. *Science*, 309(5742):1838–1841, 2005.
- [5] K. Kadau, T.C. Germann, P.S. Lomdahl, and B.L. Holian. Atomistic simulations of shock-induced transformations and their orientation dependence in bcc Fe single crystals. *Physical Review B*, 72(6):64120, 2005.
- [6] K. Kadau, TC Germann, PS Lomdahl, and BL Holian. Microscopic view of structural phase transitions induced by shock waves. *Science*, 296(5573):1681–4, 2002.
- [7] K. Kadau, T.C. Germann, P.S. Lomdahl, R.C. Albers, J.S. Wark, A. Higginbotham, and B.L. Holian. Shock Waves in Polycrystalline Iron. *Physical Review Letters*, 98(13):135701, 2007.
- [8] EM Bringa, K. Rosolankova, RE Rudd, BA Remington, JS Wark, M. Duchaineau, DH Kalantar, J. Hawreliak, and J. Belak. Shock deformation of face-centred-cubic metals on subnanosecond timescales. *Nat Mater*, 5(10):805–9, 2006.
- [9] K. Kadau, T.C. Germann, and P.S. Lomdahl. Molecular Dynamics Comes of Age: 320 Billion Atom Simulation on BlueGene/L. *International Journal of Modern Physics C*, 17(12):1755–1761, 2006.
- [10] C.L. Kelchner, SJ Plimpton, and JC Hamilton. Dislocation nucleation and defect structure during surface indentation. *Physical Review B*, 58(17):11085–11088, 1998.
- [11] DH Kalantar, JF Belak, GW Collins, JD Colvin, HM Davies, JH Eggert, TC Germann, J. Hawreliak, BL Holian, K. Kadau, et al. Direct Observation of the α - ϵ Transition in Shock-Compressed Iron via Nanosecond X-Ray Diffraction. *Physical Review Letters*, 95(7):75502, 2005.
- [12] J. Hawreliak, JD Colvin, DH Kalantar, HE Lorenzana, JS Stolken, HM Davies, TC Germann, BL Holian, K. Kadau, PS Lomdahl, et al. An Analysis of the X-Ray Diffraction Signal for the (alpha)-(epsilon) Transition in Shock-Compressed Iron: Simulation and Experiment. *Physical Review B*, 74:17, 2006.
- [13] JS Wark, D. Riley, NC Woolsey, G. Keihn, and RR Whitlock. Direct measurements of compressive and tensile strain during shock breakout by use of subnanosecond x-ray diffraction. *Journal of Applied Physics*, 68:4531, 1990.
- [14] K. Sokolowski-Tinten, C. Blome, J. Blums, A. Cavalleri, C. Dietrich, A. Tarasevitch, I. Uschmann, E. Foerster, M. Kammler, and M. Horn-von Hoegen. Femtosecond X-ray measurement of coherent lattice vibrations near the Lindemann stability limit. *Nature*, 422(6929):287–289, 2003.
- [15] H. Winick. The linac coherent light source (LCLS): a fourth-generation light source using the SLAC linac. *Journal of Electron Spectroscopy and Related Phenomena*, 75:1–8, 1995.
- [16] DT Cromer and JT Waber. International Tables for X-ray Crystallography, Vol. IV, Table 2.2 A. Birmingham: Kynoch Press. (Present distributor Kluwer Academic Publishers, Dordrecht.), pages 99–101, 1974.
- [17] D. Rez, P. Rez, and I. Grant. Dirac-Fock calculations of X-ray scattering factors and contributions to the mean inner potential for electron scattering. *Acta crystallographica. Section A, Foundations of crystallography*, 50:481–497, 1994.
- [18] JS Wark, RR Whitlock, A. Hauer, JE Swain, and PJ Solone. Shock launching in silicon studied with use of pulsed x-ray diffraction. *Physical Review B*, 35(17):9391–9394, 1987.
- [19] D.H. Kalantar. Multiple film plane diagnostic for shocked lattice measurements(invited). *Review of Scientific Instruments*, 74(3):1929, 2003.

- [20] PS Lomdahl, P. Tamayo, N. Gronbech-Jensen, and DM Beazley. 50 GFlops molecular dynamics on the Connection Machine-5. *Supercomputing'93. Proceedings*, pages 520–527, 1993.
- [21] D.M. Beazley and P.S. Lomdahl. Controlling the data glut in large-scale molecular-dynamics simulations. *Computers in Physics*, 11(3):230–238, 1997.
- [22] R.J Harrison, AF Voter, and In S.P.Chen. V. Vitek and DJ Srolovitz, Editors. *Atomistic Simulation of Materials—Beyond Pair Potentials*, page 219, 1988.
- [23] I. Ross, M. White, J. Boon, D. Craddock, A. Damerell, R. Day, A. Gibson, P. Gottfeldt, D. Nicholas, and C. Reason. Vulcan—a versatile high-power glass laser for multiuser experiments. *Quantum Electronics, IEEE Journal of*, 17(9):1653–1661, Sep 1981.
- [24] D.J. Cookson. Calculation of Absolute Intensities From X-ray Imaging Plates. *J. Synchrotron Rad.*, 5(6):1375–1382, 1998.
- [25] SG Gales and CD Bentley. Image plates as x-ray detectors in plasma physics experiments. *Review of Scientific Instruments*, 75:4001, 2004.
- [26] J. Hawreliak, HE Lorenzana, BA Remington, S. Lukezic, and JS Wark. Nanosecond x-Ray diffraction from polycrystalline and amorphous materials in a pinhole camera geometry suitable for laser shock compression experiments. *Review of Scientific Instruments*, 78:083908, 2007.
- [27] S. Plimpton. Fast parallel algorithms for short-range molecular dynamics. Technical report, SAND-91-1144, Sandia National Labs., Albuquerque, NM (United States), 1993. <http://lammps.sandia.gov>.
- [28] Y. Mishin, MJ Mehl, DA Papaconstantopoulos, AF Voter, and JD Kress. Structural stability and lattice defects in copper: Ab initio, tight-binding, and embedded-atom calculations. *Physical Review B*, 63(22):224106, 2001.
- [29] J. Li. AtomEye: an efficient atomistic configuration viewer. *Modelling and Simulation in Materials Science and Engineering*, 11(2):173–177, 2003.
- [30] B. Yaakobi, P. Bourke, Y. Conturie, J. Delettrez, JM Forsyth, RD Frankel, LM Goldman, RL McCrory, W. Seka, JM Soares, et al. High X-ray conversion efficiency with target irradiation by a frequency tripled Nd: Glass laser. *Optics Communications*, 38(3):196–200, 1981.
- [31] DL Matthews, EM Campbell, NM Ceglio, G. Hermes, R. Kauffman, L. Koppel, R. Lee, K. Manes, V. Rupert, VW Slivinsky, et al. Characterization of laser-produced plasma x-ray sources for use in x-ray radiography. *Journal of Applied Physics*, 54:4260, 1983.